Analysis of lateral diffusion from a spherical cell surface to a tubular projection

David A. Berk,* Alfred Clark, Jr.,‡ and Robert M. Hochmuth*

*Department of Mechanical Engineering and Materials Science, Duke University, Durham, North Carolina 27706; and
‡Department of Mechanical Engineering, University of Rochester, Rochester, New York 14627

ABSTRACT Cell surfaces are often heterogeneous with respect to the lateral distribution and mobility of membrane components. Because lateral mobility is related to membrane structure, measurement of a particular component's local diffusion coefficient within a distinct surface region provides useful information about the formation and maintenance of that region. Many structurally interesting cell surface features can be described as narrow tubular projections from the body of the cell. In a companion paper, we consider the thin "tethers" that can be mechanically drawn from the red blood cell membrane, and we measure the transport of fluorescent integral proteins from the surface of the cell body onto the tether. In this paper we present an analysis to describe the surface diffusion of membrane particles from a spherical shell onto a thin cylindrical process. Provision is made for different rates of diffusion within the two morphologically distinct regions. The relative role of each region in controlling the diffusive flux between regions is determined primarily by a single dimensionless parameter. This parameter incorporates the ratio of the two diffusion coefficients as well as the dimensions of each region. The analysis can be applied to a fluorescence photobleaching experiment in which the extended process is bleached. If the dimensions of the spherical cell body and the cylindrical extension are known, then the diffusion coefficients of both regions can be determined from the experimental fluorescence recovery curve.

INTRODUCTION

The experimental technique of fluorescence recovery after photobleaching (FRAP) has been used to characterize the lateral mobility of membrane components in numerous cell types. Rarely is the lateral mobility of an integral membrane protein governed by the viscosity of the lipid bilayer. Instead, protein motion is constrained by interaction with structural elements underlying the bilayer (Koppel et al., 1981; Tank et al., 1982; Wu et al., 1982). Biochemical alterations of the "membrane skeleton" can lead to changes in integral protein mobility (Golan and Veatch, 1980; Sheetz et al., 1980; Schindler et al., 1980). Thus, the measurement of lateral diffusion of integral proteins serves as an indirect but very useful probe of membrane structure.

In many cases, morphologically distinct regions of the same cell surface exhibit different rates of protein diffusion (De Laat et al., 1979; Jacobson et al., 1984; Angelides, 1986; Wolf et al., 1986). FRAP experiments involving domains within the cell surface provide important information about the structural development of the cell and the mechanisms for creating and maintaining a heterogeneous surface. The mobility of receptor proteins within local regions may be of functional significance as well.

The FRAP technique will continue to be a valuable tool for studying membrane heterogeneity. Unfortunately, as the surface domains of interest become smaller and more topologically complex, the accurate calculation of the lateral diffusion coefficient becomes increasingly problematic. In a FRAP experiment, a component of the membrane is fluorescently labeled, and a portion of the surface is bleached with intense light. The subsequent restoration of uniform fluorescence is monitored, and the diffusion coefficient is calculated from the rate of fluorescence redistribution. Most algorithms model the bleached region as a portion of an infinite plane (Axelrod et al., 1976) or a spherical shell (Huang, 1973; Koppel et al., 1980) or an ellipsoidal shell (Koppel, 1985). A single diffusion coefficient is assigned to the entire surface. In this paper we consider the case of diffusion into a bleached region that projects out from the body of the cell, forming a thin tubular process. The surface of this region is clearly distinct from the rest of the membrane in its geometric description. Furthermore, the lateral diffusion coefficients for various membrane components may have different values on this surface than on the rest of the membrane.

The extension of thin processes from a cell body is commonly observed. Various cells possess cilia, flagella, or microvilli. Other cells interact with their environment by extending "microspikes," pseudopods or filopodia. The axonal processes of nerve cells are an example of this surface geometry. The particular structure that has motivated this analysis is the red blood cell tether that forms when a red cell adheres to a surface and then is pulled away, creating a filament of membrane material between the cell body and the surface (Hochmuth et al., 1973; Evans and Hochmuth, 1976). The formation of a

tether involves the breakdown or rearrangement of normal membrane structure. In a related paper (Berk and Hochmuth, 1992), we describe a series of experiments in which the structure of tether membrane is characterized by its integral protein diffusion coefficient. In these experiments, the entire tether surface is photobleached and the subsequent return of fluorescence to that surface is measured. For the experiment to provide useful information about the tether membrane, it is necessary that the recovery process be governed by the diffusion on the tether membrane. From the theory developed here, one can (a) determine the parameter range for which this is true, and (b) derive a relationship that permits the calculation of the tether diffusion coefficient from the data.

FORMULATION

We model the cell body and its tether or process as a spherical shell of radius R_c that abruptly transforms into a cylindrical shell of radius R_T as shown in Fig. 1. The position on the spherical membrane is specified by the polar angle θ or, more conveniently, by the variable $x = \cos\theta$. At a position near $x = -1$, the surface forms a

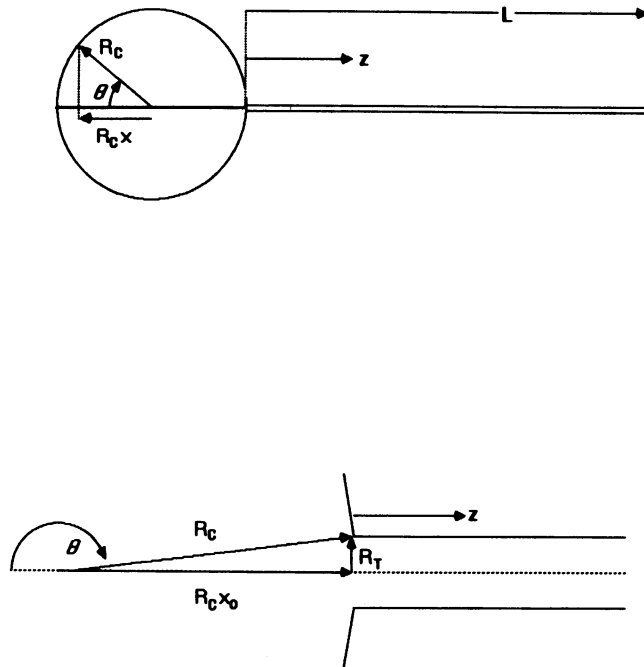FIGURE 1 A spherical surface with a cylindrical extension. On the sphere, the spatial coordinate is $x = \cos\theta$. On the projection, the coordinate is z. At the interface of sphere and cylinder, $x = -x_o, z = 0$.

cylinder. This junction is at $x = -x_o$, where

$$x_o = \sqrt{1 - (R_T^2/R_c^2)}, \qquad (1)$$

and the range of x is $-x_o \leq x \leq 1$. A position on the cylindrical surface is specified by the coordinate z. The total length of the cylinder is L. This problem is axisymmetric, so no azimuthal coordinate is required.

The surface concentration (molecules per unit area) of diffusible particles at any point on the cell body surface is denoted $N_c(x, t)$. The spherical cell body surface has a characteristic diffusion coefficient D_c, and the diffusion equation has the form:

$$\frac{\partial N_c}{\partial t} = \frac{D_c}{R_c^2} \frac{\partial}{\partial x}\left[(1 - x^2)\frac{\partial N_c}{\partial x}\right]. \qquad (2)$$

Initially, the surface concentration is uniform over the entire cell body:

$$N_c(x, 0) = N_o. \qquad (3)$$

On the membrane of the cylindrical tether, the lateral diffusion coefficient has a value D_T and the surface concentration $N_T(z, t)$ obeys the simple one-dimensional diffusion equation:

$$\frac{\partial N_T}{\partial t} = D_T \frac{\partial^2 N_T}{\partial z^2}. \qquad (4)$$

The tether is originally depleted of partices due to photobleaching:

$$N_T(z, 0) = 0. \qquad (5)$$

There can be no flow of particles past the far end of the tether, so one boundary condition is established for the cylindrical surface:

$$\frac{\partial N_T}{\partial z} = 0; \quad z = L. \qquad (6)$$

Additional boundary conditions are imposed at the interface between the cell body and tether. The concentrations and fluxes on the two surfaces must match at this point:

$$N_c(-x_o, t) = N_T(0, t) \qquad (7)$$

$$\frac{D_c}{R_c}\sqrt{1 - x^2}\frac{\partial N_c}{\partial x} = -D_T\frac{\partial N_T}{\partial z}; \quad x = -x_o, \quad z = 0. \qquad (8)$$

The total number of particles on the cylindrical surface is determined by integrating over that surface:

$$M(t) = \int_0^L 2\pi R_T N_T(z, t)\, dz. \qquad (9)$$

Another quantity of interest is the concentration at the boundary between sphere and cylinder

$$N_B(t) = N_c(-x_o, t) = N_T(0, t). \tag{10}$$

SCALING

Three dimensionless parameters appear in this problem. One parameter, x_o, has been introduced by Eq. 1. The other parameters are the square root of the diffusivity ratio,

$$\lambda = \sqrt{\frac{D_T}{D_c}}, \tag{11}$$

and the scaled tether length,

$$\ell = \frac{L}{R_c\lambda}. \tag{12}$$

We introduce the following dimensionless variables:

$$\tau = \frac{t}{R_c^2/D_c}, \tag{13a}$$

$$y = \frac{z}{R_c\lambda}, \tag{13b}$$

$$n_T = \frac{N_T}{N_o}, \tag{13c}$$

$$n_c = \frac{N_c}{N_o}. \tag{13d}$$

In dimensionless terms, the problem has the following form. On the surface of the cell body

$$\frac{\partial n_c}{\partial \tau} = \frac{\partial}{\partial x}\left[(1 - x^2)\frac{\partial n_c}{\partial x}\right], \tag{14}$$

and

$$n_c(x, 0) = 1. \tag{15}$$

On the cylindrical extension

$$\frac{\partial n_T}{\partial \tau} = \frac{\partial^2 n_T}{\partial y^2}, \tag{16}$$

$$n_T(y, 0) = 0, \tag{17}$$

and

$$\frac{\partial n_T}{\partial y} = 0, \quad y = \ell. \tag{18}$$

At the interface,

$$n_c(-x_o, \tau) = n_T(0, \tau), \tag{19}$$

and

$$\sqrt{1 - x^2}\frac{\partial n_c}{\partial x} = -\lambda\frac{\partial n_T}{\partial y}, \quad x = -x_o, \quad y = 0. \tag{20}$$

The scaled form of Eq. 9 for the total number of particles on the tether is:

$$m(\tau) = \frac{M(\tau)}{2\pi R_T L N_o} = \frac{1}{\ell}\int_0^\ell n_T(y, \tau)\, dy. \tag{21}$$

This expression gives the average concentration on the tether.

SOLUTION

We solve this problem using the LaPlace transform with respect to τ, given by

$$\bar{f}(p) = \int_0^\infty \exp(-p\tau)f(\tau)\, d\tau. \tag{22}$$

The transformed equation for the cell body is

$$p\bar{n}_c - 1 = \frac{d}{dx}\left[(1 - x^2)\frac{d\bar{n}_c}{dx}\right] \tag{23}$$

for the range $-x_o \leq x \leq 1$. The particular solution of this equation is $1/p$. The homogeneous equation is Legendre's equation, and the solution which is regular at $x = 1$ is a Legendre function of the first kind. Thus,

$$\bar{n}_c(p) = \frac{1}{p} + AP_\alpha(x), \tag{24}$$

where

$$\alpha(\alpha + 1) = -p, \tag{25}$$

with A to be determined by the boundary conditions. The transform of the cylinder portion of the problem gives

$$\bar{n}_T(p) = B\cosh[\sqrt{p}(\ell - y)]. \tag{26}$$

The LaPlace transform of the total number of particles on the cylinder is

$$\bar{m}(p) = \frac{B\sinh(\sqrt{p}\ell)}{\sqrt{p}\ell}. \tag{27}$$

The coefficients A and B are determined by the matching conditions at the boundary between the two surfaces (Eq. 19 and 20):

$$A = \frac{\lambda\sqrt{p}\tanh(\sqrt{p}\ell)}{p\sqrt{1 - x_o^2}\, P'_\alpha(-x_o)}\frac{1}{\Delta} \tag{28}$$

and

$$B = \frac{1}{p \cosh{(\sqrt{p}\ell)}} \frac{1}{\Delta} \qquad (29)$$

where

$$\Delta = 1 - \frac{P_\alpha(-x_0)\lambda\sqrt{p} \tanh{(\sqrt{p}\ell)}}{P'_\alpha(-x_0)\sqrt{1 - x_0^2}}. \qquad (30)$$

Consequently, the total number of particles on the tether is

$$\bar{m}(p) = \frac{\tanh{(\sqrt{p}\ell)}}{P^{3/2}\ell\Delta} \qquad (31)$$

and the concentration at the boundary between cell body and tether is

$$\bar{n}_B(p) = \frac{1}{p\Delta}. \qquad (32)$$

Inversion of the transform solution is accomplished by contour integration. One can show that the only singularities of the functions $\bar{m}(p)$ and $\bar{n}_B(p)$ are simple poles at $p = 0$ and at the zeros of the function Δ (see the Appendix for more details). The poles at the zeros of Δ lie on the negative real axis of the complex p plane and are denoted by

$$P_k = -\sigma_k^2/\ell^2 \qquad (33)$$

where σ_k must be determined. The inverted solution is the sum of the residues at these poles.

As shown in the Appendix, the pole $p = 0$ corresponds to the steady-state solution given by

$$\lim_{t \to \infty} m(t) = \lim_{t \to \infty} n_B(t) = \frac{R_c^2(1 + x_0)}{R_c^2(1 + x_0) + R_T L} = m_\infty. \qquad (34)$$

This is the expected result. The concentration at the boundary is equal to the average concentration, and this uniform concentration is proportional to the surface area of the cell body divided by the entire surface area, reflecting the complete redistribution of particles.

To determine the time course of the diffusional recovery, $m(t)$, the remaining residues, corresponding to zeros of the function Δ, must be calculated. Let

$$r_k = \text{Res}\left[\frac{1}{\Delta}\right]_{p = p_k}. \qquad (35)$$

Then the total number of particles on the tether can be expressed as

$$m(\tau) = m_\infty - \sum_{k=1}^{\infty} \frac{r_k \tan{\sigma_k}}{\sigma_k^3/\ell^2} \exp{[-\sigma_k^2\tau/\ell^2]} \qquad (36)$$

and the concentration at the interface is given by

$$n_B(\tau) = m_\infty - \sum_{k=1}^{\infty} \frac{r_k}{\sigma_k^2/\ell^2} \exp{[-\sigma_k^2\tau/\ell^2]}. \qquad (37)$$

The values of σ_k can be calculated by exploiting the fact that $(1 - x_0)$ is small. As detailed in the Appendix, the accumulation of particles on the tether surface for all but very short times $(t \sim R_T^2/D_c)$ is described by

$$m(t) = m_\infty - \sum_{k=1}^{K} a_k \exp{[-\sigma_k^2 D_T t/L^2]} \qquad (38)$$

where

$$a_k = \frac{2\beta^2}{\sigma_k^2(\beta + \beta^2 + \sigma_k^2)} \qquad (39)$$

and

$$\beta = \frac{D_c}{D_T} \frac{L}{R_T\ell n\,[2R_c/R_T]}. \qquad (40)$$

The values of σ_k are the roots of

$$\sigma_k \tan{\sigma_k} = \beta. \qquad (41)$$

The upper limit of the sum is

$$K \cong \frac{L}{\pi R_T\lambda}. \qquad (42)$$

The concentration at the interface is given by an equation identical to Eq. 38 except that the coefficient a_k is replaced by

$$b_k = \frac{2\beta}{\beta + \beta^2 + \sigma_k^2}. \qquad (43)$$

In these equations, the previously defined dimensionless time and length have been recast in their dimensional form.

Note that when diffusion on the cell body is very fast $(D_T/D_c \to 0)$, the term β approaches infinity, σ_k approaches $(2k - 1)\pi/2$, and a_k approaches $(2/\sigma_k^2)$. In this limit the solution is independent of D_c.

At the other extreme, when β is very small due to slow diffusion on the cell body $(D_T/D_c \to \infty)$, the higher order terms in Eq. 38 vanish. For the first term, Eq. 41 simplifies to $\sigma_1^2 = \beta$. The simplified solution is

$$m(t) = m_\infty - \exp{\left[\frac{-D_c t}{R_T L \ell n(2R_c/R_T)}\right]} \qquad (44)$$

The tether dimensions appear in this solution, but the diffusivity in the tether D_T, does not.

Regardless of the value for β, there is a large portion

of time in which the solution is adequately expressed using only the first term of the series, $k = 1$, in Eq. 38. In Fig. 2, a logarithmic plot of σ_1^2 vs. β reveals the relative importance of cell body and tether to the recovery process. When β is large, σ_1^2 is a constant $(\pi^2/4)$, indicating that the dimensionless time tD_T/L^2 is appropriate and that recovery times are independent of D_c. When β is small σ_1^2 and β are linearly related, indicating that the recovery time is independent of D_T and properly scaled as $tD_c/[R_T L\ell n(2R_c/R_T)]$, instead. In between these two extremes is a transition region in which both D_T and D_c have a significant effect on the recovery time.

DISCUSSION

This analysis finds its application in the design of a fluorescence recovery experiment involving a thin membrane process. A particular geometry can be evaluted to determine whether the measured recovery rate can be used to calculate the diffusivity on the membrane process. Fig. 3 illustrates this concept by separating the material and geometric variables of Eq. 40, which defines β. The line represented by $\beta = 1$ divides the

FIGURE 3 Effects of dimensions and diffusivities. The ratio of the two diffusion coefficients and the geometry of the surfaces determine which surface controls the flux from cell body to tether. In the region $\beta > 1$, the rate of diffusion is sensitive to the tether diffusion coefficient D_T.
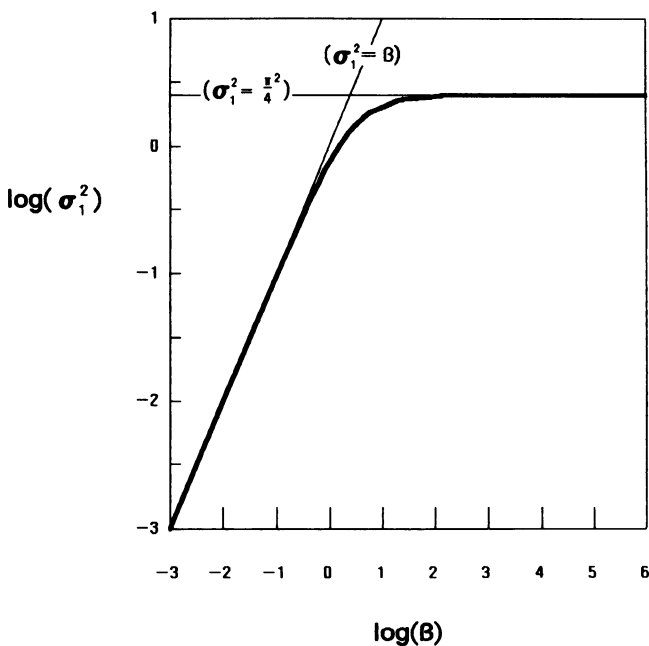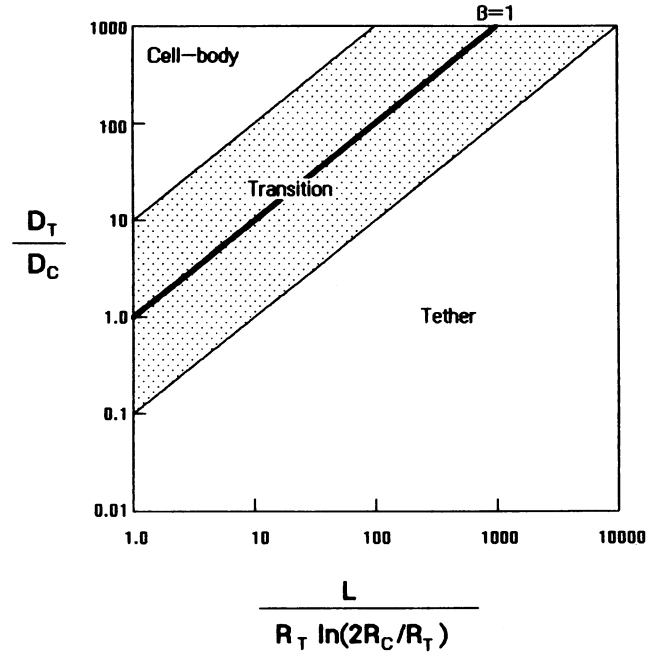

FIGURE 2 Dependence of σ_1^2 on the parameter β. The timescale of diffusive transport from cell body to tether is $L^2/(\sigma_1^2 D_T)$. In the region of constant slope, $[R_T L\ell n(2R_c/R_T)]/D_c$ is the appropriate time scale. In the region of zero slope, L^2/D_T is the proper scale. In the transition region, the diffusivities of both surfaces affect the diffusive flux.

tether- and cell body-dominated regimes. For example, given a cell body radius of 3 μm, a tether radius of 0.05 μm, and a tether length of 1 μm, ratios of $D_T/D_c > 4$ fall within the "cell-body zone." Thus, even if it is suspected that the diffusivity on the tether membrane is greater than that on the cell body, it will be difficult to detect this increase in diffusivity. It will be impossible to distinguish between a ten-fold and hundred-fold increase in D_T relative to D_c. However, if the tether in this example were drawn out to a length of 25 μm or more, then the recovery time would depend on the tether membrane diffusivity even when its value is two orders of magnitude greater than the value of the cell body.

A tether photobleaching experiment seems feasible based on an expected ratio of diffusion coefficients, but in the general case neither coefficient value is known. We assume that the geometric parameters are known. Although the radius of the process in many cases is below the limits of resolution of a light microscope, a reliable measurement may be obtained by direct measurement using electron microsopy or by an indirect method (Hochmuth et al., 1983). The cell body diffusion coefficient may be determined by a separate FRAP

experiment (for instance, by bleaching a spot on the cell body surface away from the process). If D_c is known, then the remaining coefficient can be determined using a straightforward iterative scheme.

In the absence of an independent measurement of D_c, it may be possible to resolve both coefficients from the same fluorescence recovery curve $F(t)$. Given a set of data for the recovery of fluorescence, including the final steady-state value F_∞, the rate of recovery is predicted by

$$S(t) = 1 - \frac{F(t) - F(o)}{F_\infty - F(o)} = 1 - \frac{m(t)}{m_\infty}. \tag{45}$$

A semilog plot of the experimental values for $S(t)$ should reveal a large linear region described by:

$$\ell n S = \ell n \left\{ \left(1 + \frac{R_T L}{2 R_c^2}\right) \frac{2\beta^2}{\sigma_1^2[\sigma_1^2 + \beta^2 + \beta]} \right\} - (\sigma_1^2 D_T / L^2)t \tag{46}$$

From the intercept and slope the two diffusion coefficients can be calculated. It should be emphasized that this method is useful only when the values for the two diffusivities are approximately equal. When the recovery is dominated by only one of the surfaces, the coefficient of the other surface will be highly sensitive to small changes in the regression line fitted to the data and therefore unmeasurable for that experiment.

This analysis shows that in many cases it is feasible to measure the lateral diffusion coefficient on the membrane of a tubular process by photobleaching the entire process and measuring the recovery of fluorescence. The feasibility of this experiment is favored by a long process length, a narrow process radius and a slow diffusion on the process as compared to the cell body surface. Of course there are many circumstances in which other photobleaching techniques are possible. When the process is sufficiently long, a spot or pattern photobleaching approach is preferable (Koppel et al., 1986). However, there are a number of situations in which this technique of bleaching the whole process may be useful. If the process only extends one or two microns, then a laser-illuminated spot will cover the entire structure. It may also be necessary to illuminate the entire process to get a measurable signal if the fluorescent labeling of the surface is weak. Finally, bleaching the entire process makes it possible to use a conventional light source in place of laser illumination in certain cases. Because the recovery time of a long cylinder of membrane is much larger than that associated with micron-size laser-bleached spots, a conventional light soure (arc lamp) can photobleach the membrane over the course of several seconds rather than over milliseconds.

APPENDIX

Inversion of LaPlace transform solution

The steady-state solution for both the average and boundary concentration is obtained from Eqs. 31 or 32 as

$$r_o = \lim_{p \to 0} \frac{1}{\Delta}, \tag{A1}$$

where the function Δ is given by Eq. 30. From Eq. 25, α approaches $-p$ as $p \to 0$; therefore,

$$\lim_{p \to 0} P_\alpha(-x_o) = P_o(-x_o) = 1. \tag{A2}$$

From the recurrence relation

$$P'_\alpha(z) = \frac{\alpha[z P_\alpha(z) - P_{\alpha-1}(z)]}{z^2 - 1} \tag{A3}$$

it can be shown that for small values of α,

$$P'_\alpha(z) = \frac{\alpha(z - 1) P_o(z)}{z^2 - 1} = \frac{\alpha}{z + 1}, \tag{A4}$$

and, therefore,

$$\lim_{p \to 0} = \frac{P_\alpha(-x_o)}{P'_\alpha(-x_o)} = -\frac{1 - x_o}{P}. \tag{A5}$$

It now follows that

$$\lim_{p \to 0} \Delta = 1 + \lambda \ell \frac{1 - x_o}{1 + x_o}, \tag{A6}$$

and the steady state solution is

$$m_\infty = \frac{(1 + x_o)}{(1 + x_o) + \lambda \ell \sqrt{1 - x_o^2}}. \tag{A7}$$

This is the dimensionless form of the result given by Eq. 34.

Additional terms for the transient portion of the solution correspond to zeros of the function Δ, as expressed in Eqs. 35–37. At this point, we introduce the assumption that x_o is close to one by replacing the Legendre function and its derivative with the following asymptotic expressions (Lebedev, 1965):

$$P_\alpha(-x_o) \approx \frac{\sin \alpha \pi}{\pi} \ell n \left[\frac{1 - x_o}{2}\right], \tag{A8}$$

$$P'_\alpha(-x_o) \approx \frac{\sin \alpha \pi}{\pi} \ell n \left[\frac{1}{1 - x_o}\right]. \tag{A9}$$

Thus

$$\frac{P_\alpha(-x_o)}{P'_\alpha(-x_o) \, 1 - x_o^2} \approx \sqrt{\frac{1 - x_o}{1 + x_o}} \, \ell n \left[\frac{1 - x_o}{2}\right]$$

$$\approx \sqrt{\frac{1 - x_o}{2}} \, \ell n \left[\frac{1 - x_o}{2}\right]. \tag{A10}$$

In terms of cell dimensions,

$$x_o \approx 1 - \frac{R_T^2}{2R_c^2}, \tag{A11}$$

and the approximation becomes:

$$\frac{P_\alpha(-x_o)}{P'_\alpha(-x_o)\sqrt{1-x_o^2}} \approx \frac{R_T}{R_c}\ell n\left[\frac{R_T}{2R_c}\right]. \tag{A12}$$

The function Δ is now given by:

$$\Delta \approx 1 - \lambda(R_T/R_c)\,\ell n\,(R_T/2R_c)\,\sqrt{p}\,\tanh\,(\sqrt{p}\ell) \tag{A13}$$

and its zeros $(p_k = -\sigma_k^2/\ell^2)$ must satisfy

$$\sigma_k \tan \sigma_k = \beta \tag{A14}$$

with

$$\beta = \frac{L}{\lambda^2 R_T \ell n(2R_C/R_T)}. \tag{A15}$$

The residue defined in Eq. 35 is

$$r_k = \text{Res}\,[1/\Delta]_{p=p_k} = \frac{2\beta\sigma_k^2}{\ell^2[\beta + \beta^2 + \sigma_k^2]}. \tag{A16}$$

from which follow the solutions given by Eqs. 38 and 43.

The approximations given in Eqs. A8 and A9 are not uniformly valid for all values of α. Using formulas developed by Hobson (1931), it can be shown that a better approximation for P_α is

$$P_\alpha(-x_o) = \frac{\sin \alpha\pi}{\pi}(C_1 + C_2) \tag{A17}$$

$$C_1 = \ln\left(\frac{1-x_o}{2}\right) + 2\psi(1+\alpha) + \cot \alpha\pi + 2\gamma \tag{A18}$$

$$C_2 = \frac{1-x_o}{2}\left(-\alpha(\alpha+1)\,\ell n\left(\frac{1-x_o}{2}\right)\right.$$
$$\left. - \alpha(\alpha+1)\,[2\psi(\alpha+1) + \cot \alpha\pi + 2\gamma]\right) \tag{A19}$$

where ψ is the Digamma function and γ is Euler's constant. For large values of α the second term C_2 becomes significant when

$$(1 - x_o)\alpha^2 \sim 1. \tag{A20}$$

When α (and p) is sufficiently large, the simple approximation of Eqs. A8 and A9 breaks down. Thus, the upper limit K in the approximate solution, Eq. 38, is determined by $(1 - x_o)\alpha^2 \sim 1$, or $(1 - x_o)p \sim 1$. From Eqs. 33 and A9 we get the restriction

$$\sigma_k < \sigma_K = \frac{R_C}{R_T}\ell. \tag{A21}$$

Eq. 41 implies that for large k, σ_k approaches $\pi(k-1)$, so the acceptable values of k are given by

$$k < K = \frac{R_c\ell}{R_T\pi}. \tag{A22}$$

REFERENCES

Angelides, K. J. 1986. Fluorescently labelled Na$^+$ channels are localized and immobilized to synapses of innervated muscle fibres. *Nature (Lond.).* 321:63–66.

Axelrod, D., D. E. Koppel, J. Schlessinger, E. Elson, and W. W. Webb. 1976. Mobility measurement by analysis of fluorescence photobleaching recovery kinetics. *Biophys. J.* 16:1055–1069.

Berk, D. A., and R. M. Hochmuth. 1992. Lateral mobility of integral proteins in red blood cell tethers. *Biophys. J.* 61:9–18.

De Laat, S. W., P. T. van der Saag, E. L. Elson, and J. Schlessinger. 1979. Lateral diffusion of membrane lipids and proteins is increased specifically in neurites of differentiating neuroblastoma cells. *Biochim. Biophys. Acta.* 558:247–250.

Evans, E. A., and R. M. Hochmuth. 1976. Membrane viscoplastic flow. *Biophys. J.* 16:13–26.

Golan, D. E., and W. Veatch. 1980. Lateral mobility of band 3 in the human erythrocyte membrane studied by fluorescence photobleaching recovery: Evidence for control by cytoskeletal interactions. *Proc. Natl. Acad. Sci. USA.* 77:2537–2541.

Hobson, E. W. 1931. The Theory of Spherical and Ellipsoidal Harmonics. Cambridge University Press. 225 pp.

Hochmuth, R. M., N. Mohandas, and P. L. Blackshear. 1973. Measurement of the elastic modulus for red cell membrane using a fluid mechanical technique. *Biophys. J.* 13:747–762.

Hochmuth, R. M., E. A. Evans, H. C. Wiles, and J. T. McCown. 1983. Mechanical measurement of red cell membrane thickness. *Science (Wash., DC).* 220:101–102.

Huang, H. W. 1973. Mobility and diffusion in the plane of cell membrane. *J. Theor. Biol.* 40:11–17.

Jacobson, K., D. O'Dell, and J. T. August. 1984. Lateral diffusion of an 80,000-D glycoprotein in the plasma membrane of murine fibroblasts: Relationships to cell structure and function. *J. Cell Biol.* 99:1624–1633.

Koppel, D. E. 1985. Normal-mode analysis of lateral diffusion on a bounded membrane surface. *Biophys. J.* 47:337–347.

Koppel, D. E., M. P. Sheetz, and M. Schindler. 1980. Lateral diffusion in biological membranes: A normal-mode analysis of diffusion on a spherical surface. *Biophys. J.* 30:187–192.

Koppel, D. E., M. P. Sheetz, and M. Schindler. 1981. Matrix control of protein diffusion in biological membranes. *Proc. Natl. Acad. Sci. USA.* 78:3576–3580.

Koppel, D. E., P. Primakoff, and D. G. Myles. 1986. Fluorescence photobleaching analysis of cell surface regionalization. *In* Applications of Fluorescence in the Biomedical Sciences. D. L. Taylor, A. S. Waggoner, F. Lanni, R. F. Murphy, and R. R. Birge, editors. Alan R. Liss, Inc. 477–497.

Lebedev, N. N. 1965. Special Functions and their Applications. Prentice Hall, Englewood Cliffs, NJ. 201 pp.

Schindler, M., D. E. Koppel, and M. P. Sheetz. 1980. Modulation of

membrane protein lateral mobility by polyphosphates and poly-amines. *Proc. Natl. Acad. Sci. USA.* 77:1457–1461.

Sheetz, M. P., M. Schindler, and D. E. Koppel. 1980. Lateral mobility of integral membrane proteins is increased in spherocytic erythrocytes. *Nature (Lond.).* 285:510–512.

Tank, D. W., E. S. Wu, and W. W. Webb. 1982. Enhanced molecular diffusibility in muscle membrane blebs: release of lateral constraints. *J. Cell Biol.* 92:207–212.

Wolf, D. E., S. S. Hagopian, R. G. Lewis, J. K. Voglmayr, and G. Fairbanks. 1986. Lateral regionalization and diffusion of a maturation-dependent antigen in the ram sperm plasma membrane. *J. Cell Biol.* 102:1826–1831.

Wu, E. S., D. W. Tank, and W. W. Webb. 1982. Unconstrained lateral diffusion of concanavalin A receptors on bulbous lymphocytes. *Proc. Natl. Acad. Sci. USA.* 79:4962–4966.